Sensors & Diagnostics

PAPER

View Article Online
View Journal | View Issue

Cite this: *Sens. Diagn.*, 2025, **4**, 529

Sensitive electrochemical detection of DR1 based on gold nanoparticle-modified MoS_2 and hyaluronic acid-based thionine

Yaping Zhang, †[a] Gao Si,†[c] Zhendong Wang,[a] Yilong Wang,[a] Xiaojing Cui,[a] Huaixia Yang, *[a] Fuchun Si*[b] and Yanjiu Liu *[a]

The analysis of down-regulator of transcription 1 (DR1) offers significant information for the rapid and non-invasive diagnosis of Hashimoto's thyroiditis (HT). In this study, we report a novel dual-signal amplification electrochemical biosensor for the sensitive detection of DR1. Gold nanoparticle (AuNP)-modified molybdenum disulfide (MoS_2@AuNPs), which has extremely strong electron transfer ability and abundant binding sites, is first modified on an electrode surface as a substrate material to implement the first signal amplification. After the formation of the sandwich structure based on the specific recognition of antigens and antibodies, the electroactive molecules hyaluronic acid-based thionine (HA@Thi) are introduced to achieve the second signal amplification. Using this dual-signal amplification strategy, the proposed biosensor achieves a linear range of 1×10^{-4}–1×10^{2} ng mL^{-1} with a low detection limit of 10.99 fg mL^{-1}. In addition, the electrochemical biosensor has high selectivity and good stability, and is applicable to the assay of DR1 in the presence of complex biological matrices, which is expected to provide a scientific approach for the clinical application of serum DR1 monitoring. More importantly, our method may extend the application of protein-based biosensors in disease diagnosis techniques.

Received 16th August 2024,
Accepted 1st October 2024

DOI: 10.1039/d4sd00286e

rsc.li/sensors

1. Introduction

Hashimoto's thyroiditis (HT) is one of the most common thyroid diseases. In recent years, the incidence of HT combined with thyroid cancer is increasing, and has developed into a serious threat to human health and quality of life.[1] The onset of HT is insidious, and the establishment of sensitive and efficient early diagnosis systems is the most effective means to treat HT. Down-regulator of transcription 1 (DR1) can be used as a specific marker of HT. Therefore, highly sensitive and accurate detection of DR1 is very important for early diagnosis and monitoring of disease progression.

Electrochemical sensors are real-time detection devices that integrate a recognition element and a conducting element, which can perform qualitative and quantitative analysis of the target.[2,3] In recent years, electrochemical sensors have been widely used in rapid detection of target molecules and clinical medicine diagnosis,[4] because of their inherent advantages, such as high sensitivity, strong selectivity, and rapid response.[5] Researchers are committed to further improving the detection sensitivity of electrochemical sensors to enable them to meet the needs of low concentration biomarker detection in the early stage of disease.[6,7] Currently, various signal amplification strategies have been used in biosensing systems, including nanomaterials,[8] polymerization,[9] enzyme catalysis,[10] *etc.* Among them, nanomaterials have gradually received widespread attention due to their high specific surface area, high electrical conductivity, and good biocompatibility.[11–14]

Molybdenum disulfide (MoS_2) is a transition metal dichalcogenide, which comprises a layer of transition metal atoms sandwiched between two layers of chalcogen atoms and have attracted extensive attention owing to their extraordinary properties and potential applications.[15–19] For example, Shuai *et al.* constructed an ultrasensitive electrochemical biosensor for detecting microRNAs based on hollow MoS_2 microcubes. Under optimum conditions, the proposed biosensor has a detection limit of 0.086 fM.[19] Monolayer MoS_2, as a new kind of ultrathin two-dimensional layered transition metal material, has more superior properties such as abundant storage, good

[a] *Pharmacy College, Henan University of Chinese Medicine, Zhengzhou 450046, P. R. China. E-mail: yanghuaixia886@163.com, liuyanju886@163.com*
[b] *Henan Provincial Key Laboratory of Prescription-Syndrome Signal Transduction of Traditional Chinese Medicine, International Joint Laboratory of Prescription-Syndrome Signal Transduction of Traditional Chinese Medicine in Henan Province, Henan University of Chinese Medicine, Zhengzhou 450046, P. R. China. E-mail: sifc2000@hotmail.com*
[c] *Department of Orthopedic, Peking University Third Hospital, Beijing 100191, P. R. China*
† These authors contributed equally.

mechanical strength, large surface area and easy functionalization,[20–23] which make it highly attractive in sensing applications. However, studies have found that compared with single metal oxides, noble metal nanoparticle-modified metal oxides have higher electrochemical activity.[24] Gold nanoparticles (AuNPs) are commonly used functional nanomaterials with good chemical stability, high surface area, and fast electron transfer properties.[25,26] More importantly, AuNPs can stably bind proteins without changing their biological activities.[27] The AuNP-modified MoS_2 (MoS_2@AuNPs) nanocomposite has excellent electrochemical performance and can be used to significantly improve the sensitivity of a sensor.

Hyaluronic acid (HA), the simplest glycosaminoglycan (GAG) found in nature, is a polymer formed by linking disaccharide units of D-glucuronic acid (GlcUA) to *N*-acetyl-D-glucosamine (GlcNAc).[28,29] As a high molecular weight linear mucopolysaccharide with high stability and excellent biocompatibility, HA is widely used in cosmetics, pharmaceuticals and other fields.[30,31] Thionine (Thi) is a highly electrically active substance, which can produce a strong electrical signal when labeled on an electrode surface, and is widely used in the field of electrochemical sensing.[32] Applying the complex HA and Thi (HA@Thi) to the sensor can greatly increase the number of binding signal molecules and improve the sensitivity of the electrochemical sensor.

In this study, a novel dual-signal amplification biosensor based on MoS_2@AuNPs and HA@Thi for sensitive detection of DR1 was developed. The nanocomposite MoS_2@AuNPs with a large specific surface area and high conductivity was first modified on the electrode surface to achieve the first signal amplification. Subsequently, a sandwich structure was formed by adding antibody 1 (Ab1), DR1 and antibody 2 (Ab2) on the electrode surface through specific recognition of antigens and antibodies to ensure the specificity of the sensor. Finally, a large number of electroactive molecules Thi were modified on the electrode surface by esterification of HA and Ab2, which significantly improved the detection sensitivity of this electrochemical sensor. Under optimal conditions, this biosensor exhibited a wide detection range of 1×10^{-4}–1×10^{2} ng mL^{-1} and a low detection limit of 10.99 fg mL^{-1}. At present, there are few studies on the direct detection of DR1 in serum by electrochemistry; thus, this highly sensitive detection strategy contributes to clinical research on the progression of HT and other diseases, which demonstrates its high potential application in clinical diagnosis.

2. Materials and methods

Antibody 1 and antibody 2 were purchased from Sangon Biotechnology Co., Ltd. (Shanghai, China). Down-regulator of transcription 1 (DR1) was bought from Cloud Cloning Technology Co., Ltd. Tetrachloroauric acid ($HAuCl_4$) was obtained from Shanghai Aladdin Biochemical Technology Co., Ltd. (Shanghai, China). Human troponin I-cardiac (cTnI) and human epidermal growth factor receptor 2 (HER2) were supplied by Shanghai Linc-Bio Science Co., Ltd. (Shanghai, China). Carcinoembryonic antigen (CEA) and cytokeratin fragment antigen 21-1 (CY 21-1) were purchased from Shanghai Sangon Biotechnology Co., Ltd. (Shanghai, China). Tris-HCl buffer and sodium citrate were purchased from Shanghai Sangon Biotechnology Co., Ltd. (Shanghai, China). Hyaluronic acid (HA), thionine (Thi) and bovine serum albumin (BSA) were obtained from Sigma-Aldrich Trading Co., Ltd. (Shanghai, China). Monolayer molybdenum disulfide (MoS_2) nanosheets were provided by our cooperator Dr. Wang, and the details of MoS_2 can be seen in his previously reported article.[33]

All reagents were analytical grade. The seven clinical samples were provided by the Third Affiliated Hospital of Henan University of Traditional Chinese Medicine. All experiments were performed in accordance with the Guidelines "International Ethical Guidelines for Biomedical Research Involving Human Subjects", and approved by the ethics committee of Henan Provincial Hospital of Traditional Chinese Medicine. Informed consents were obtained from human participants of this study.

2.1. Apparatus

Electrochemical experiments including cyclic voltammetry (CV) and square wave voltammetry (SWV) were carried out on a RST5200F electrochemical workstation (Zhengzhou Risetest Electronic Co. Ltd., China). A conventional three-electrode system consisting of a modified glassy carbon electrode (3 mm in diameter), a saturated calomel electrode, and a platinum wire control electrode was used during the experiments. The surface morphology of the electrode was characterized using a Sigma 500 scanning electron microscope (SEM) and an FEI Talos F200X G2 transmission electron microscope (TEM). Electrochemical impedance spectra (EIS) were scanned and recorded on an Autolab PGSTAT M204 electrochemical workstation (the electrolyte solution was 5 mM $[Fe(CN)_6]^{3-/4-}$ solution containing 0.1 M KNO_3, frequency range: 0.1 Hz–0.1 MHz, alternating voltage: 5 mV, amplitude: 0.005 Hz).

2.2. Preparation of AuNP composites

Firstly, $HAuCl_4$ aqueous solution (10 mL, 1 mM) was added to a round-bottom flask and heated with constant stirring until boiling. Then, 2 mL of trisodium citrate aqueous solution (38.8 mM) was quickly added and continued to maintain the boiling state until the color of the solution no longer change. Finally, the heat source was removed, and the AuNPs were cooled to room temperature with continuous stirring and stored at 4 °C away from light.

2.3. Preparation of MoS_2@AuNP composites

0.005 g MoS_2 was dispersed in 10 mL of anhydrous ethanol and sonicated for 2 h to obtain uniformly dispersed nanosheets. Then, the prepared AuNP solution was mixed

with MoS_2 dispersion solution in equal volume and sonicated for 30 min to obtain MoS_2@AuNP nanocomposites.[34]

2.4. Fabrication of the electrochemical biosensor

Prior to use, the glassy carbon electrode (GCE) was mechanically polished with 0.3 μm Al_2O_3 powder to obtain a smooth and flat electrode surface. After that, the electrode was scanned by cyclic voltammetry (CV) (scanning range: −0.2–0.6 V) in a glassy carbon electrode cleaning solution (1 mM $K_3Fe(CN)_4$, 0.2 M KNO_3), until the potential difference of the redox peak on the cyclic voltammetry curve was less than 80 mV. Then, the scanned electrodes were ultrasonically cleaned (1 min each time) with ultrapure water, anhydrous ethanol, and ultrapure water in sequence and dried in a stream of nitrogen. Subsequently, 4 μL of MoS_2@AuNP suspension was added to the electrode surface and dried at 37 °C for 20 min, allowing the nanomaterials to be modified on the electrode surface by electrostatic adsorption (MoS_2@AuNPs/GCE). And then 5 μL of Ab1 solution (1 μg mL^{-1}) was added to the electrode surface and incubated overnight at 37 °C (Ab1/MoS_2@AuNPs/GCE). Whereafter, the unbound Ab1 on the electrode surface was rinsed with ultrapure water and blown dry with nitrogen. Therewith, the electrode was immersed in 1% bovine serum albumin (BSA) solution and reacted at 37 °C for 30 min to fully seal the unspecifically bound sites (BSA/Ab1/MoS_2@AuNPs/GCE). Subsequently, 5 μL of DR1 (1 ng mL^{-1}) solution was added dropwise to the modified electrodes and incubated for 1 h at 37 °C. After rinsing the unbound DR1 on the electrode surface with ultrapure water and drying the electrode with nitrogen (DR1/BSA/Ab1/MoS_2@AuNPs/GCE), 5 μL of Ab2 solution (1 μg mL^{-1}) was added dropwise on the electrode surface, and the reaction was carried out at 37 °C for 1 h (Ab2/DR1/BSA/Ab1/MoS_2@AuNPs/GCE). After incubation, the unbound Ab2 on the electrode surface was rinsed with ultrapure water and blown dry with nitrogen. Subsequently, the electrode was immersed in the activated HA@Thi solution and reacted at 37 °C for 1 h (HA@Thi/Ab2/DR1/BSA/Ab1/MoS_2@AuNPs/GCE), whereas the fully modified electrode was later moderately washed with ultrapure water and blown dry with nitrogen.

The fully modified electrode was immersed in Tris-HCl buffer with pH = 7, and electrochemical tests were carried out by square wave voltammetry (SWV) to record the response signal of the current, and the concentration of DR1 was

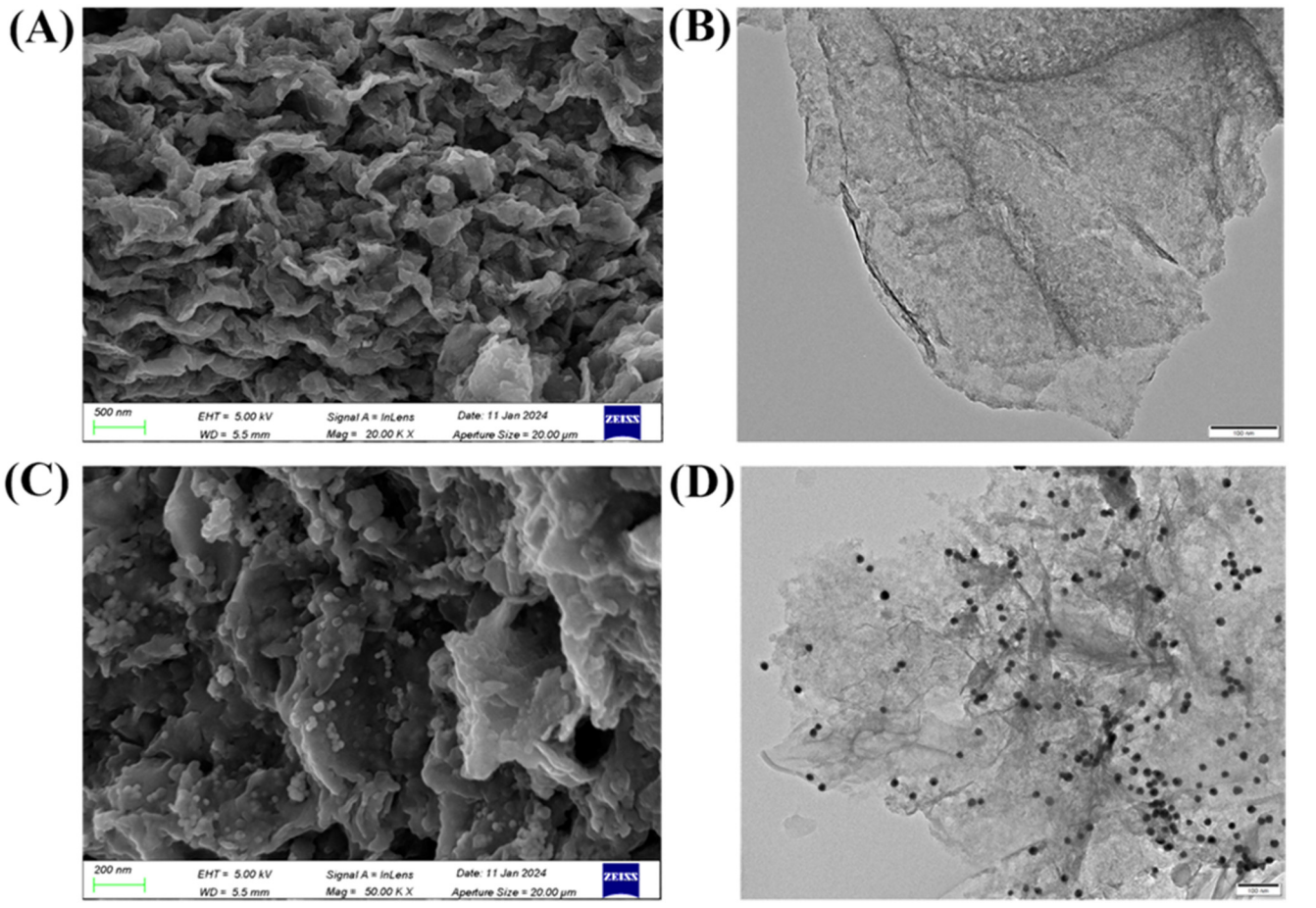

Fig. 1 SEM (A) and TEM (B) images of MoS_2 nanosheets. SEM (C) and TEM (D) images of MoS_2@AuNP nanocomposites.

determined and analyzed according to the intensity of the redox current (scanning range: −0.6–0.2 V).

3. Results and discussion

3.1. Characterization of MoS_2 and MoS_2@AuNPs

The morphology of MoS_2 nanosheets was characterized by scanning electron microscopy (SEM) (Fig. 1A) and transmission electron microscopy (TEM) (Fig. 1B). Fig. 1A presents the obvious lamellar structure of MoS_2. Fig. 1B shows that MoS_2 has a monolayer lamellar structure with low symmetry. This structure of MoS_2 shows its high specific surface area and could provide more binding sites for the modifier. Besides, the surface morphology of MoS_2@AuNP nanocomposites was also characterized by SEM (Fig. 1C) and TEM (Fig. 1D). Fig. 1C and D both show that MoS_2 in the complex maintained the original flaky structure, and AuNPs were uniformly distributed on the MoS_2 nanosheets. All these results indicated that MoS_2@AuNP nanocomposites have been successfully prepared.

3.2. Principles of the DR1 biosensor based on MoS_2@AuNPs and HA@Thi

In this study, a dual-signal amplification biosensor for sensitive detection of DR1 was constructed. Scheme 1 shows the detection principle of this electrochemical sensor for DR1. MoS_2@AuNP nanocomposites with extreme electron transfer ability and abundant binding sites were first modified as substrate materials on the electrode surface to form a stable and dense electron-conducting active layer, which could improve the electrochemical performance of the electrode and the probe loading, achieving the first signal amplification. After that, the biorecognition probe Ab1 was connected to the electrode surface by forming a gold–ammonia bond with the AuNPs, and the unbound non-specific sites on the electrode surface were sealed with the blocking agent BSA. Whereafter, a sandwich structure was formed by adding DR1 and Ab2 successively. The specific combination of the antigen and antibody ensured the high selectivity of the sensor. Then, the carboxyl group of HA was activated by EDC/NHS to a succinimidyl ester structure, which was highly reactive with the amino group of Ab2 and thus attached to the electrode surface. The electroactive molecule Thi was grafted onto the electrode surface in large quantities *via* HA, leading to the second signal amplification and thus greatly improved the detection sensitivity of this sensor.

3.3. Feasibility analysis

In this part of the experiment, the different modified electrodes were used to detect DR1 and their electrochemical signals were compared to analyze the feasibility of this electrochemical biosensor for DR1 detection. As shown in Fig. 2, for the fully modified electrode, a significant current signal could be observed at around −0.23 V (curve g). However, for the incomplete modified electrodes, including the electrodes without modification using MoS_2@AuNPs (curve a), Ab1 (curve b), DR1 (curve c), Ab2 (curve d), HA (curve e) and Thi (curve f), there was no significant current response. These experimental results showed that the electrochemical biosensor was feasible for DR1 detection and that the biosensor could not be successfully constructed when either step was missing.

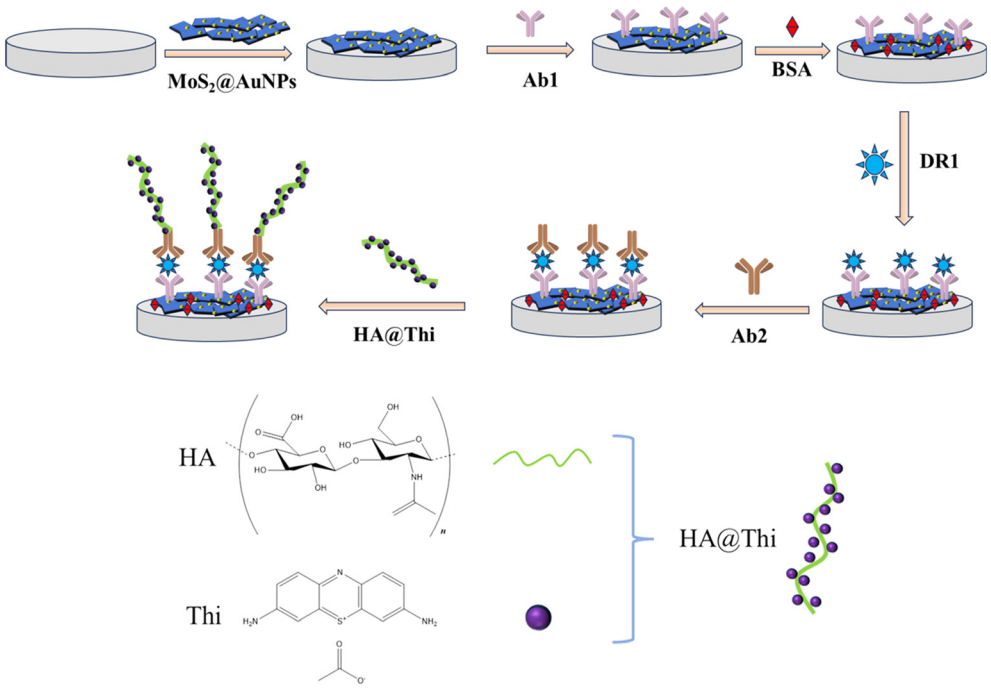

Scheme 1 Scheme diagram of the dual-signal amplification electrochemical biosensor based on MoS_2@AuNPs and HA@Thi for DR1 detection.

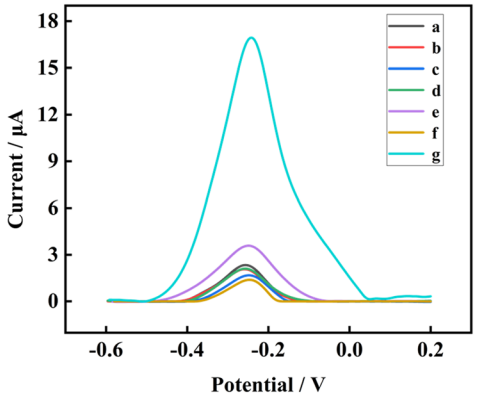

Fig. 2 SWV signal response curves of the electrochemical biosensor after modification with all the components (MoS_2@AuNPs/Ab1/DR1/Ab2/HA/Thi) (g), and without MoS_2@AuNPs (a), Ab1 (b), DR1 (c), Ab2 (d), HA (e), and Thi (f) modification.

3.4. Electrochemical characterization of the biosensor

The electrochemical performance of the stepwise modified electrodes was evaluated by electrochemical impedance spectroscopy (EIS), which is sensitive to the change of the solid–liquid interface. According to the Nyquist plots, the semicircle diameter in the high frequency region represents the charge transfer resistance (R_{ct}) on the electrode surface, which corresponds to the charge transfer kinetics of the $[Fe(CN)_6]^{4-/3-}$ probe on the electrode surface. Fig. 3A shows the Nyquist plots of the electrode layer-by-layer assembly process. Compared with bare GCE (~242.15 Ω, curve a), the R_{ct} decreased when MoS_2@AuNPs were modified on the electrode surface (~183.87 Ω, curve b). This was mainly due to the excellent electrical conductivity of MoS_2@AuNP nanocomposites, which could accelerate the electron transport rate at the electrode surface, resulting in a decrease in resistance. The amino group of Ab1 was bound to the electrode surface by forming gold–ammonia bonds with the AuNPs, leading to an increase in R_{ct} (~429.69 Ω, curve c). After BSA modification, the unspecifically bound sites on the electrode surface were closed, forming a dense film on the electrode surface and the R_{ct} increased to ~810.73 Ω (curve d). When DR1 was captured by the antibody on the electrode surface, the R_{ct} further increased to ~1140.5 Ω (curve e), which was attributed to the gradual increase of spatial site resistance on the electrode surface, inhibiting the electron transfer of the redox probe. Subsequently, Ab2 was attached to the electrode surface by specifically recognizing DR1, which further increased the R_{ct} (~1610.2 Ω, curve f). Then, the modification of HA@Thi on the electrode surface introduced a large number of electroactive molecules to aggregate on the electrode surface, which greatly increased the spatial site resistance of the electrode surface thus hindering the interfacial charge transfer, and the R_{ct} further increased to ~2153.7 Ω (curve g). The above experimental results showed that the stepwise modification of this electrochemical sensor was successful.

In addition, the electrochemical performance of the stepwise modified electrodes was further characterized by cyclic voltammetry (CV). The results are shown in Fig. 3B, and compared with bare GCE (curve a), the modification of MoS_2@AuNPs accelerated the electron transport rate on the electrode surface and made the current intensity increase sharply (curve b). However, with the gradual modification of Ab1, BSA, DR1, Ab2, and HA@Thi on the electrode, the charge transfer at the electrode interface was gradually inhibited, leading to a gradual decrease in the current intensity (curve c–curve g). The results of CV were consistent with those of EIS, indicating that the stepwise modification of the sensor was successful.

3.5. Optimization of experimental conditions

To achieve the best analytical performance of the sensing system, the key conditions during the sensor construction process, including the modification amount of MoS_2@AuNPs,

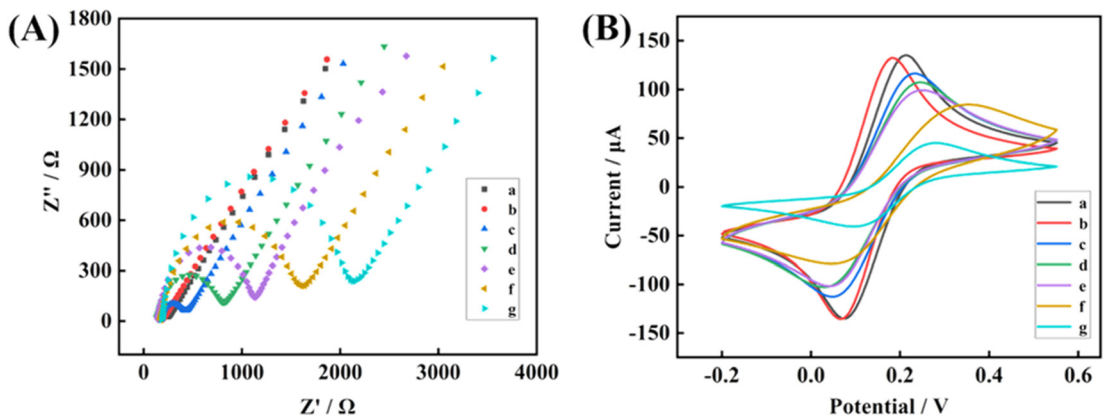

Fig. 3 EIS (A) and CV (B) profiles of layer-by-layer modified electrodes GCE (a), MoS_2@AuNPs/GCE (b), Ab1/MoS_2@AuNPs/GCE (c), BSA/Ab1/MoS_2@AuNPs/GCE (d), DR1/BSA/Ab1/MoS_2@AuNPs/GCE (e), Ab2/DR1/BSA/Ab1/MoS_2@AuNPs/GCE (f), and HA@Thi/Ab2/DR1/BSA/Ab1/MoS_2@AuNPs/GCE (g).

the volume ratio of HA to Thi, and the reaction time of HA@Thi, were optimized.

The extent to which the nanocomposites form a conductive film on the electrode surface was closely related to the performance of the biosensor. Therefore, the relationship between the modification amount of the MoS_2@AuNP nanocomposite and the current response strength of the sensor was investigated. As can be seen from Fig. 4A, the current intensity gradually increased with the increase of nanocomposite modification volume and reached the maximum value at 4 μL. When the modification amount of nanomaterials was more than 4 μL, the current intensity was almost unchanged, which is probably because the amount of nanomaterials adsorbed on the electrode surface reached saturation. Therefore, the optimal modification volume of nanocomposites in this experiment was 4 μL.

Thi is an important electrochemical signal molecule, and the volume ratio of Thi to HA is closely related to the number of modified signal molecules on the electrode surface. Therefore, the effect of volume ratio of Thi to HA on the current signal intensity of the biosensor was investigated. As shown in Fig. 4B, as the volume ratio of Thi to HA was increased from 1 : 1 to 20 : 1, the current intensity gradually increased. However, when the volume ratio of Thi to HA exceeded 20 : 1, the current signal of the sensing system no longer change significantly; this might be due to the effect of spatial site resistance, which made the binding efficiency of signal molecules on the electrode surface gradually decrease. Therefore, the optimal volume ratio of Thi to HA was 20 : 1.

Moreover, the effect of reaction time of HA@Thi on the current intensity of electrochemical biosensors was researched. Theoretically, a longer reaction time is more conducive to the enrichment of electroactive signaling molecules on the electrode surface, while this will reduce the efficiency of the sensor in practical applications. Thus, the changes of electrochemical signal response with the reaction time of HA@Thi from 15 to 90 min were investigated. From Fig. 4C, we can find that the current intensity gradually increased with the increase of HA@Thi reaction time in the first 60 min, and when the reaction time continued to increase, the current intensity remained basically unchanged. This might be attributed to the fact that the reaction has reached equilibrium at 60 min and the reaction rate was limited; therefore, the optimal reaction time for HA@Thi was set at 60 min.

3.6. Analytical performance of the sensor

The linear range and detection limit are important parameters to evaluate the analytical detection performance as well as the practical application potential of the sensor. Therefore, the electrochemical response ability of the sensor to different concentrations of DR1 was studied to evaluate the analytical performance of the sensor. As shown in Fig. 5A, the SWV curve has a clear current signal around −0.23 V, corresponding to the peak position of the electrochemical signal molecule Thi. With the increase of DR1 concentration from 1×10^{-4} ng mL^{-1} to 1×10^{2} ng mL^{-1}, the peak current increased gradually. And there was a good linear relationship between the peak current and the logarithm of the DR1 concentration in the range of 1×10^{-4} ng mL^{-1} to 1×10^{2} ng mL^{-1} (Fig. 5B); the linear regression equation was I (μA) = 5.10367 × lg(C_{DR1}) + 10.4249 (R^2 = 0.998), and a low detection limit (LOD) of 10.99 fg mL^{-1} was calculated (S/N = 3, where S is the standard deviation of the blank measurements (n = 5) and N is the slope of the regression equation). The above results indicated that the biosensor was highly sensitive and could detect trace amounts of DR1 with high sensitivity over a wide detection range. Furthermore, we compared the analytical performance of this sensor with those of other reported sensors (Table 1), and the results showed that this sensor is better than or close to previously reported studies, which is of great significance for practical application.

3.7. Selectivity, reproducibility and stability

Selectivity is an important index to evaluate the performance of biosensors in identifying target molecules. Therefore, the current signal response values of this sensor to different biomarkers with the same concentration, including cardiac

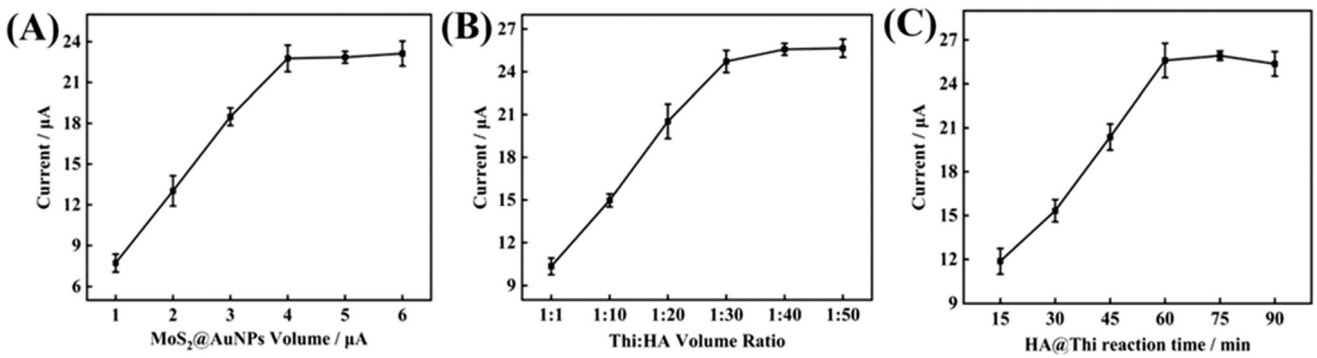

Fig. 4 Effect of (A) the amount of MoS_2@AuNP nanocomposites, (B) the volume ratio of Thi to HA, and (C) the reaction time of HA@Thi on the peak current (error bars indicate the standard deviation of three replicate parallel experiments, and all DR1 samples were at a concentration of 1 ng mL^{-1}).

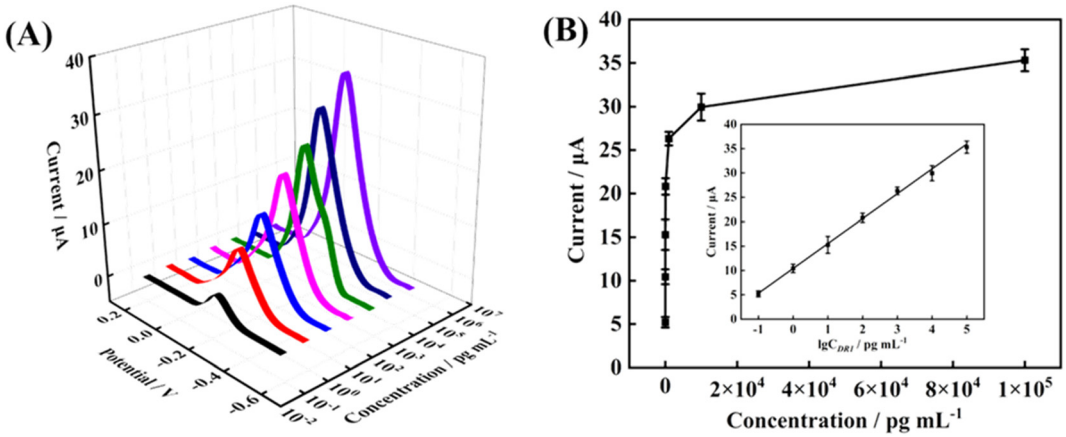

Fig. 5 (A) SWV response curves of the biosensor to different concentrations of DR1. (B) Fitted curve of the logarithm of DR1 concentration *versus* current response intensity (error bars indicate the standard deviation of three replicate parallel experiments).

Table 1 Comparison of this biosensor with other reported biosensors

Analyte	Sensor types	Linear range	Detection limit	Ref.
DR1	Electrochemical sensor	5×10^{-4}–5×10^{2} ng mL^{-1}	0.159 pg mL^{-1}	9
DR1	Electrochemical sensor	1×10^{-4}–1×10^{2} ng mL^{-1}	2.91 fg mL^{-1}	35
Human enterovirus 71	Electrochemical sensor	1.0–0.01 ng mL^{-1}	0.01 ng mL^{-1}	36
Tetracycline	Electrochemical sensor	0.05–100 ng mL^{-1}	8.8 pg mL^{-1}	37
DR1	Electrochemical sensor	1×10^{-4}–1×10^{2} ng mL^{-1}	10.99 fg mL^{-1}	This work

troponin I (cTnI), cytokeratin fragment antigen 21-1 (CY21-1), carcinoembryonic antigen (CEA), and human epidermal growth factor receptor 2 (HER2), were measured under the same experimental conditions, and their results were compared with that of DR1 to evaluate the selectivity of the biosensor. As can be seen from Fig. 6A, the electrochemical response values of cTnI, CY 21-1, CEA, and HER2 were much lower than that of DR1, and their peak currents were 9.16%, 8.41%, 7.45%, and 8.48% of that of DR1, respectively. When DR1 was mixed with the four interfering species, its electrochemical signal could still reach 86.33%. These results showed that this method has good selectivity for the detection of DR1 in complex environments.

The anti-interference ability is also an important indicator of the clinical application potential of the analysis method. Therefore, to evaluate the anti-interference ability of this method in detecting DR1, the DR1 samples were diluted to different concentrations with 5% and 10% human serum, respectively, and their oxidation current signals were measured using this biosensor and compared with those of DR1 samples with the same concentration in PBS buffer solution. As shown in Fig. 6B, for 100 fg mL^{-1} DR1 samples in 5% and 10% human serum, the electrochemical signals were 97.62% and 88.12% of that in PBS buffer, respectively. For 100 pg mL^{-1} DR1 samples in 5% and 10% human serum, the electrochemical signals were 86.34% and 92.34% of that in PBS buffer, respectively. For

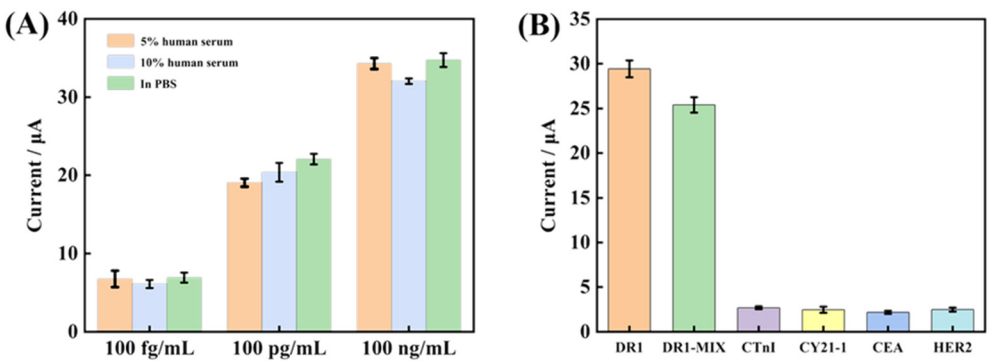

Fig. 6 (A) Current response of different concentrations of DR1 in 5% and 10% human serum interference matrices and in PBS buffer, respectively. (B) Selectivity study of the constructed sensor for DR1 detection.

Table 2 Comparison of the detection results of this sensor with those of ELISA kits

Sample	Electrochemical method (fg mL^{-1})	ELISA (fg mL^{-1})	Relative error (%)
1	587.77	617.7	−4.85
2	426.28	419.1	+1.71
3	175.43	169.5	+3.5
4	1514.54	1546.6	−2.07
5	1477.43	1421.6	+3.93
6	198.15	196.9	+0.79
7	220.02	230.5	−4.55

100 ng mL^{-1} DR1 samples in 5% and 10% human serum, the electrochemical signals were 98.73% and 92.29% of that in PBS buffer, respectively. The above results indicated that the biosensor has strong anti-interference ability and great potential for clinical application.

To estimate the stability of the constructed sensors, three groups of sensors with identical modifications were prepared under the same experimental conditions; one group was measured instantly, and the other two groups were stored in a constant temperature refrigerator at 4 °C and took out for measurement after 2 and 4 weeks, respectively. The experimental results showed that 95.21% of the electrochemical signal was retained after 2 weeks of storage, and 90.20% of the electrochemical signal was retained after 4 weeks of storage (n = 5), indicating that the sensor has good stability. In addition, to ensure the reliability of this sensor for DR1 detection, the reproducibility of this sensor was investigated based on intra- and inter-group experiments. The relative standard deviation (RSD) of the intra- and inter-group experimental results were 3.41% and 3.87% (n = 3), respectively, demonstrating that the constructed electrochemical sensors has good reproducibility.

3.8. Detection of clinical serum samples

In order to investigate the reliability of this electrochemical sensing method in the detection of clinical samples, the proposed method was applied to the detection of actual samples, and the results were compared with the detection data of the ELISA kit. As shown in Table 2, the detection results of the constructed sensor were highly consistent with those of the ELISA kits, and the relative error (RE) was less than ±5%, which indicated that the constructed electrochemical sensor has good reliability in the detection of clinical samples, and it has potential practical application prospect.

The seven clinical samples were provided by the Third Affiliated Hospital of Henan University of Traditional Chinese Medicine and used without further treatment.

4. Conclusion

In conclusion, an electrochemical sensor based on MoS_2@AuNP nanomaterials and HA@Thi signaling molecules was constructed for efficient, facile, and ultrasensitive detection of DR1. MoS_2@AuNPs increased the conductivity of the electrode while also providing a large number of active sites for biomolecules, achieving the first signal amplification. HA@Thi as a signal molecule was attached to the electrode surface in large quantities to realize the second signal amplification. Through the dual-signal amplification strategy, the sensor could detect DR1 with an LOD of 10.99 fg mL^{-1}. In addition, the electrochemical biosensor has the advantages of high sensitivity, good selectivity and stability, and is also suitable for the detection of DR1 in complex biological matrices. The proposed method might be extended for the analysis of other biomarkers by replacing different antigens and antibodies, and has promising clinical application prospect. However, few studies have been reported on the electrochemical detection of DR1, and it is still a challenge to realize real clinical application, which will be the direction of our future work.

Data availability

While we are committed to transparency and publishing the details of the method used in this work, we are constrained by a patent proprietary agreement to publish raw data and code.

Conflicts of interest

There are no conflicts to declare.

Acknowledgements

This work was supported by the Project of Tackling of Key Scientific and Technical Problems in Henan Province (232102321119) and Henan Provincial Science and Technology R&D Program Joint Fund (222301420024).

References

1 Q. Y. Zhang, X. P. Ye, Z. Zhou, C. F. Zhu, R. Li, Y. Fang, R. J. Zhang, L. Li, W. Liu, Z. Wang, S. Y. Song, S. Y. Lu, S. X. Zhao, J. N. Lin and H. D. Song, *Nat. Commun.*, 2022, **13**, 775, DOI: **10.1038/s41467-022-28120-2**.

2 Z. Zhou, S. Mukherjee, S. Hou, W. Li, M. Elsner and R. A. Fischer, *Angew. Chem., Int. Ed.*, 2021, **60**, 20551–20557, DOI: **10.1002/anie.202107860**.

3 Z. X. Liu, Z. D. Wang, L. L. Ma, L. Guo, H. X. Yang, Y. J. Liu and M. S. Miao, Programmable target-driven MNAzyme and DNA tetrahedron framework synergistically constructed label-free electrochemical sensing platform for TMV RNA detection, *Sens. Actuators, B*, 2025, **428**, 137526, DOI: **10.1016/j.snb.2025.137256**.

4 T. Y. Gao, Z. B. Zhou, D. Cheng, Y. J. Liu, H. X. Yang and Y. Wang, Electrochemical biosensor for highly sensitive detection of cTnI based on a dual signal amplification strategy of ARGET ATRP and ROP, *Talanta*, 2024, **266**, 125009, DOI: **10.1016/j.talanta.2023.125009**.

5 S. Sarwar, M. C. Lin, C. Amezaga, Z. Wei, E. Iyayi, H. Polk, R. G. Wang, H. H. Wang and X. Y. Zhang, *Adv. Compos. Hybrid Mater.*, 2023, **6**, 49, DOI: **10.1007/s42114-023-00630-7**.

6 J. Y. Shi, S. Y. Liu, P. Y. Li, Y. Lin, H. Luo, Y. Y. Wu, J. Yan, K. J. Huang and X. C. Tan, *Biosens. Bioelectron.*, 2023, **237**, 115557, DOI: **10.1016/j.bios.2023.115557**.

7 L. Y. Zhao, H. X. Yang, X. K. Zheng, J. G. Li, L. H. Jian, W. S. Feng and J. M. Kong, Dual signal amplification by polysaccharide and eATRP for ultrasensitive detection of CYFRA 21–1 DNA, *Biosens. Bioelectron.*, 2020, **150**, 111895–115230, DOI: **10.1016/j.bios.2019.111895**.

8 J. Yang, R. Z. Zhang, J. X. Liu, R. B. Xiong, Y. He, X. J. Luo and X. Yang, *Food Chem.*, 2024, **454**, 139806, DOI: **10.1016/j.foodchem.2024.139806**.

9 F. C. Si, X. J. Cui, Y. P. Zhang, Y. F. Li, H. X. Yang and Y. J. Liu, *Sens. Actuators, B*, 2024, **403**, 135080, DOI: **10.1016/j.snb.2023.135080**.

10 H. Wan, X. Q. Wang and J. Cheng, *ACS Nano*, 2022, **16**, 14849–14859, DOI: **10.1021/acsnano.2c05752**.

11 X. H. He, W. Y. Zhang, Y. L. Wang, Z. D. Wang, J. F. Wang, X. F. Li, H. X. Yang, Y. J. Liu and M. S. Miao, Synergistic signal amplification for HER2 biosensing using tetrahedral DNA nanostructures and 2D transition metal carbon/nitride@Au composites via ARGET ATRP, *Microchem. J.*, 2024, **207**, 112029, DOI: **10.1016/j.microc.2024.112029**.

12 K. K. Reddy, H. Bandal, M. Satyanarayana, K. Y. Goud, K. V. Gobi, T. Jayaramudu, J. Amalraj and H. Kim, *Adv. Sci.*, 2020, **7**, 1902980, DOI: **10.1002/advs.201902980**.

13 T. Dong, N. M. Matos Pires, Z. Yang and Z. Jiang, *Adv. Sci.*, 2023, **10**, 2205429, DOI: **10.1002/advs.202205429**.

14 X. Wang, G. Zhang, W. Yin, S. Zheng, Q. Kong, J. Tian and H. Pang, *Carbon Energy*, 2022, **4**, 246–281, DOI: **10.1002/cey2.182**.

15 X. Li, X. Sun, H. Yu, H. Li, X. Sun, X. Tao and Y. Zheng, *Appl. Catal., B*, 2022, **307**, 21156, DOI: **10.1016/j.apcatb.2022.121156**.

16 X. Wang, Y. W. Zhang, H. N. Si, Q. H. Zhang, J. Wu, L. Gao, X. F. Wei, Y. Sun, Q. L. Liao, Z. Zhang, K. Ammarah, L. Gu, Z. Kang and Y. Zhang, *J. Am. Chem. Soc.*, 2020, **142**, 4298–4308, DOI: **10.1021/jacs.9b12113**.

17 S. Roy, K. A. Deo, K. A. Singh, H. P. Lee, A. Jaiswal and A. K. Gaharwar, *Adv. Drug Delivery Rev.*, 2022, **187**, 114361, DOI: **10.1016/j.addr.2022.1143**.

18 K. J. Huang, Y. J. Liu, H. B. Wang, Y. Y. Wang and Y. M. Liu, *Biosens. Bioelectron.*, 2014, **55**, 195–202, DOI: **10.1016/j.bios.2013.11.061**.

19 H. L. Shuai, K. J. Huang, Y. X. Chen, L. X. Fang and M. P. Jia, *Biosens. Bioelectron.*, 2017, **89**, 989–997, DOI: **10.1016/j.bios.2016.10.051**.

20 L. Sun, B. Javvaji, C. Zhang, X. Zhuang and W. Chen, *Nano Energy*, 2022, **102**, 107701, DOI: **10.1016/j.nanoen.2022.107701**.

21 S. Chen, Y. Sun, Y. Xia, K. Lv, B. Man and C. Yang, *Biosens. Bioelectron.*, 2020, **156**, 112128, DOI: **10.1016/j.bios.2020.112128**.

22 Y. Li, Y. Zhang, X. Tong, X. Wang, L. Zhang, X. Xia and J. Tu, *J. Mater. Chem. A*, 2021, **9**, 1418–1428, DOI: **10.1039/D0TA08514F**.

23 G. Wei, J. Wei, J. Zhou, Y. Chen, D. Wu and Q. Wang, *Chem. Eng. J.*, 2020, **382**, 123018, DOI: **10.1016/j.cej.2019.123018**.

24 S. Sawan, R. Maalouf, A. Errachid and N. Jaffrezic-Renault, *TrAC, Trends Anal. Chem.*, 2020, **131**, 116014, DOI: **10.1016/j.trac.2020.116014**.

25 L. Guo, S. J. Zhou, J. Y. Xue, Z. H. Liu, S. Q. Xu, Z. X. He and H. X. Yang, Signal-enhanced electrochemical sensor employing MWCNTs/CMK-3/ AuNPs and Au@Pd core–shell structure for sensitive determination of AFB1 in complex matrix, *Microchim. Acta*, 2024, **191**, 594–5598, DOI: **10.1007/s00604-024-06665-x**.

26 A. Jahangiri-Manesh, M. Mousazadeh, S. Taji, A. Bahmani, A. Zarepour, A. Zarrabi, E. Sharifi and M. Azimzadeh, *Pharmaceutics*, 2022, **14**, 664, DOI: **10.3390/pharmaceutics14030664**.

27 J. Ou, H. Tan, X. Chen and Z. Chen, *Nanomaterials*, 2018, **8**, 994, DOI: **10.3390/nano8120994**.

28 A. Passi and D. Vigetti, *Adv. Drug Delivery Rev.*, 2019, **146**, 83–96, DOI: **10.1016/j.addr.2019.08.006**.

29 A. Parnigoni, P. Moretto, M. Viola, E. Karousou, A. Passi and D. Vigetti, *Cancers*, 2023, **15**, 3813, DOI: **10.3390/cancers15153813**.

30 A. Nazeri, A. Niazi, A. Afsharifar, S. Taghavi, A. Moghadam and F. Aram, *Sci. Rep.*, 2021, **11**, 17966, DOI: **10.1038/s41598-021-97139-0**.

31 H. Deng, J. Wang and R. An, *Front. Pharmacol.*, 2023, **14**, 1131001, DOI: **10.3389/fphar.2023.1131001**.

32 R. Hallaj, Z. Ghafary, O. Kamal Mohammed and R. Shakeri, *Biosens. Bioelectron.*, 2023, **227**, 115168, DOI: **10.1016/j.bios.2023.115168**.

33 D. Wang, H. Li, N. Du, Z. Lang, T. Hu and W. Hou, *J. Colloid Interface Sci.*, 2019, **541**, 183–191, DOI: **10.1016/j.jcis.2019.01.079**.

34 J. Wu, Y. Lu, Z. Wu, S. Li, Q. Zhang, Z. Chen, J. Jiang, S. Lin, L. Zhu, C. Li and Q. Liu, *Sens. Actuators, B*, 2018, **261**, 279–287, DOI: **10.1016/j.snb.2018.01.166**.

35 X. J. Cui, Y. P. Zhang, H. M. Zhang, H. X. Yang, Y. J. Liu and F. C. Si, *New J. Chem.*, 2024, **48**, 8106–8115, DOI: **10.1039/d4nj01098a**.

36 Y. H. Hou, J. J. Wang, Y. Z. Jiang, C. Lv, L. Xia, S. L. Hong, M. Lin, Y. Lin, Z. L. Zhang and D. W. Pang, *Biosens. Bioelectron.*, 2018, **99**, 186–192, DOI: **10.1016/j.bios.2017.07.035**.

37 Q. Y. Wu, C. Zhang, L. Z. Yi, X. J. Fan, Y. Gu and S. Wang, *Sens. Actuators, B*, 2024, **419**, 136411, DOI: **10.1016/j.snb.2024.136411**.